Penerbit Akademia Baru

Journal of Advanced Research in Fluid Mechanics and Thermal Sciences

Journal homepage: www.akademiabaru.com/arfmts.html
ISSN: 2289-7879

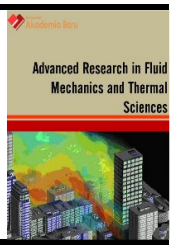

Kinematic and Computational Fluid Dynamics Analysis of an Underwater Manipulator Arm in Streamline and Blunt Body Arrangement

Open Access

Ahmad Anas Yusof[1,*], Mohd Khairi Mohamad Nor[1], Shamsul Anuar Shamsudin[1], Mohd Rizal Alkahari[1]

[1] Faculty of Mechanical Engineering, Universiti Teknikal Malaysia Melaka, Hand Tuah Jaya, 76100 Durian Tunggal, Melaka, Malaysia

ARTICLE INFO

Article history:
Received 13 February 2018
Received in revised form 26 April 2018
Accepted 2 June 2018
Available online 23 July 2018

ABSTRACT

This paper presents the hydrodynamic modeling, simulation and analysis of kinematic, velocity vector and pressure distribution of an underwater manipulator arm designed for a remotely operated underwater vehicle. The focus is to improve the modeling accuracy of the arm, which is simulated in a streamline and blunt body arrangement, with extended and retracted position, in order to achieve better control for coordinated motion of the 5 degree of freedom manipulator arm. The arm is simulated in suspended and submerged scenario, above and underwater, respectively. Kinematic analysis of the manipulator has been studied in order to identify the workspace of the manipulator. The workspace is important as it will define the working area suitable to be developed on the test rig, in order to study the effectiveness of using the manipulator arm for underwater application. Velocity vector and pressure distribution analysis is conducted in a laminar flow condition with a velocity of 0.1 m/s, which is in the range for underwater cases. The manipulator arm model is defined as the static body in a moving fluid. For retracted and extended condition which have been set according to the streamlines of inlet velocity on z-axis direction, high pressure occur at the arm, the tips of the gripper holder and model base as it exposed to the fluid flow and velocity. In the blunt body arrangement, pressure build up is discovered in most of the body cross section that exposed to the flow.

Keywords:
Underwater Manipulator, ROV, AUV, CFD, Kinematic Analysis

Copyright © 2018 PENERBIT AKADEMIA BARU - All rights reserved

1. Introduction

Underwater manipulators enable underwater vehicles to out operations for ocean-based activities. It provides the important function by imitating the function of human arm in carrying underwater drilling, cutting, pick-and-place task and even assembling parts. Thus, the manipulator is regarded as the important elements for remotely operated vehicles (ROVs) or autonomous underwater vehicles (AUVs) in ocean exploration, construction, inspection, and recovery operation. Until today, underwater manipulator has come in different sizes, shapes and functions for ocean

* *Corresponding author.*
E-mail address: anas@utem.edu.my (Ahmad Anas Yusof)

applications [1-5]. Figure 1 illustrates the use of an underwater manipulator on a ROV. The overall performance of underwater manipulation is greatly affected by the hydrodynamic forces exerted by the surrounding fluid. The interaction with the water environment will eventually influence the performance of the position and motion control of the end-effector/gripper during task manipulation on the respected target position. Thus, in underwater senario, the impact of the environment cannot be neglected, in determining controllability of the system and the consequence of the surrounding hydrodynamic forces [6].

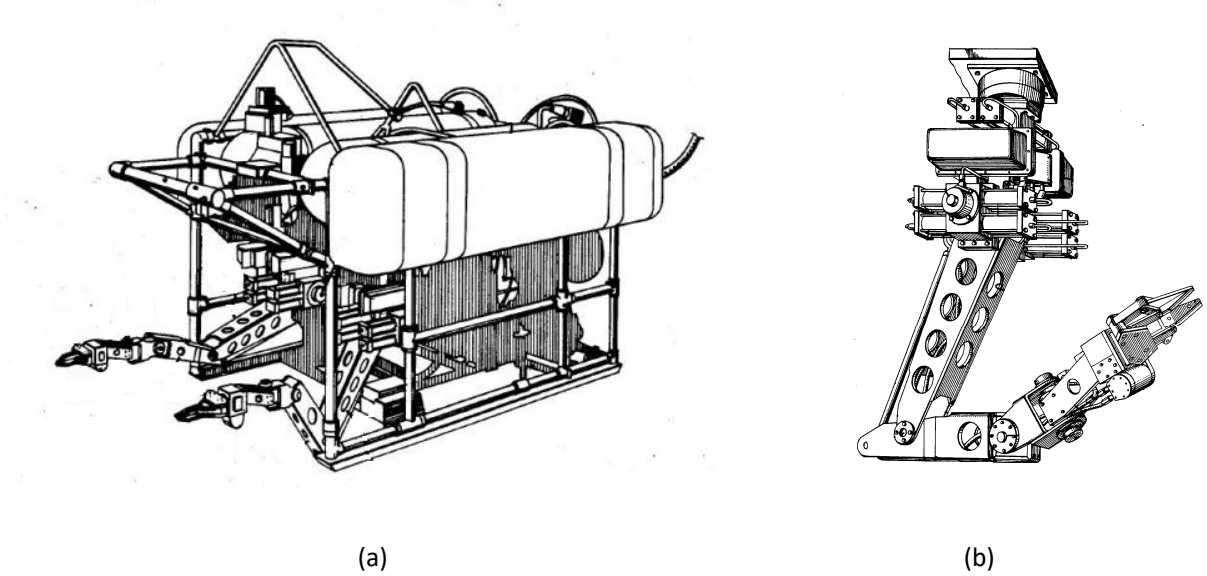

(a) (b)

Fig. 1. (a) Underwater Manipulator Arm on an Remotely Operated Underwater Vehicle (b) Manipulator Arm [1]

Flow directions and waves represent important conditions in the uncertain underwater environment. Ocean currents are caused by many factors, which include wind velocities, tidal movements, ocean themals and salinity, and the Coriolis force due to the Earth rotation. Furthermore, real ocean currents are often multi-directional and irregular, spatially and time variable, producing significant disturbance to the underwater manipulator. [7]. Underwater robotic manipulators with unlimited workspace and mobility create complex motion planning and difficult control algorith, which require high redundancy and strong uncertainty analysis. Most researchers prepare groundwork for the underwater research on control schemes based on the the mathematical representation built by using the Denavit-Hartenberg (D-H) method [8,9]. Other than that, the geometry of the manipulator has been studied by establishing the direct and inverse kinematics. Then, the dynamic model is developed and used by employing the Lagrange theorem. Furthermore, derivation, computer simulation and mechanical system dynamics analysis can be accomplished using the MATLAB and ADAMS software [10].

Experimental analysis of the hydrodynamic forces and torque that act on the underwater manipulator has been studied by Mclain and Rock [11]. Basically, the higly rotational and accelerative motions of the end effect of the manipulator results in the three-dimensional transient flow. The complex transient flow generate large hydrodynamic forces that are difficult to model accurately. A standard method at that time is to model a two-dimensional analysis of a circular cylinder that moved unsteadily in an incompressible, inviscid and stationary fluid, with discrete vortices trailing the cylinder. This model was extended into 3D regime using strip theory. The experiment include added

mass analysis and drag coefficient from position, velocity, acceleration and torque measurement. The interaction effects due to the dynamic coupling between the vehicle and the manipulator has been investigated by Santhakumar [12] using closed-form equations which provide a generalized scheme for formulating the equations of motion of the underwater manipulator. The proposed scheme makes it possible to identify the structure, nature, and properties of the system, and it simplifies the control design. His study also proposed a model reference control approach for an underactuated underwater manipulator in retracted to perform underwater intervention tasks incorporating desired trajectory information. Extensive simulations were carried out to verify and demonstrate the effectiveness of the proposed scheme using Forward and Inverse Kinematics, as well as Dynamic Model of the Underwater Manipulator.

In the latest development of autonomous manipulator system, Filaretova and Konoplina [13] has designed a method of synthesis of system of automatic correction of program trajectory of motion of multilink manipulator installed on underwater vehicle. The system allows of fast and high quality problem solving and underwater manipulation operations performance with less operator supervision. This improve operator resistance to fatigue during manipulator operation.

In this paper, we are going to address the kinematics model of the manipulator, by investigating its polar coordinate systems and inverse kinematics analysis to acquire the optimum work space for the manipulator. Computational fluid dynamics FLUENT simulation is conducted to verify the flow disturbance on the underwater manipulator, in forward and sideward force. This will put the manipulator in a streamline and blunt object arrangement. The pressure distribution and velocity vector on the manipulator with respect to streamline and blunt object arrangement, and submerged or suspended condition is also investigated in the simulation.

2. Methodology

An immersed moving solid body in an ocean flow will be subjected to the pressure and shear stress distributions resulting from their relative movement. Kinematic and computational fluid dynamics (CFD) analysis is conducted on the proposed manipulator, by subjecting it with modeling and simulation of workspace trajectory, velocity vector and pressure distribution. In the equations of kinematic analysis, motion of the manipulator joints, shown in Figure 2, is usually not affected by the effect of velocity and pressure distribution. This effect will however be closedly studied in the CFD analysis of the manipulator in selected manipulator cases and condition, with preset boundary condition, as shown in Figure 3.

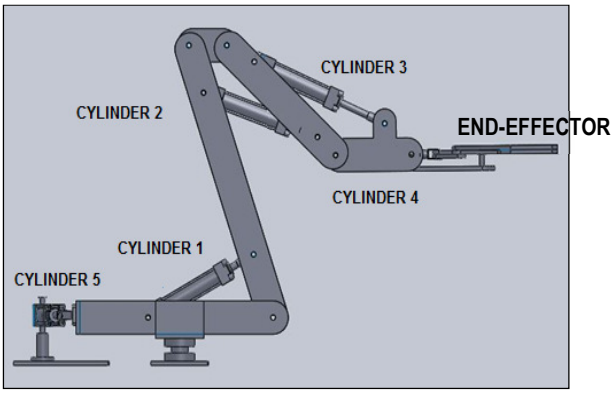

Fig. 2. Manipulator Arm Joints and Links for Kinematic Analysis

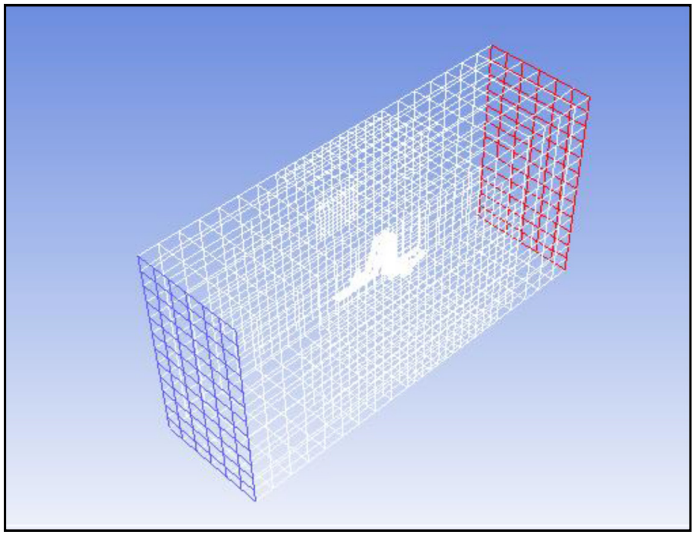

Fig. 3. Manipulator Arm Boundary Condition for CFD Analysis

The CFD analysis is based on several conditions, which is the position of the manipulator arm relative to the angle of the arm, its location in the simulation whether facing the ocean current or not and the scenario mode in which it is suspended in the air or submerged underwater for different type of fluid analysis. Table 1 shows the manipulator simulation conditions for all scenario and arrangement.

Table 1
Manipulator Simulation Conditions

Manipulator simulation conditions	
Manipulator	Retracted or Extended
Scenario Mode	Suspended or Submerged
Arrangement	Streamline or Blunt

Figure 4 and 5 show the retracted manipulator and the extended manipulator condition according to the preset angle purposely chosen for the CFD analysis. The angle is shown in Table 2. Suspended scenario refers to the manipulator being simulated in the air, while submerged scenario refers to the underwater analysis. Laminar flow is used in the simulation, by assuming that the manipulator is operated in a slow movement.

Figure 6 shows the typical drag coefficient and Reynold numbers for some streamline and blunt body. In the analysis, streamline arrangement is created whereby the manipulator is facing the flow according to the concept of streamline body. In streamline body, viscosity is assumed to have negligible effects on lift and moment, and this is only valid only for streamline bodies which gradually taper to a point or sharp edge and are roughly aligned with the ocean free stream flow direction. [15]. Blunt arrangement is where the manipulator is set with the flow from the left or right side, where the faces are blunter or having more cross-sectional area. Viscosity is assumed to play more important role for all the forces and moments. Such flows exhibit flow separation, which is the sudden thickening or breakaway of the boundary layer from the surface, resulting in a thick trailing wake.

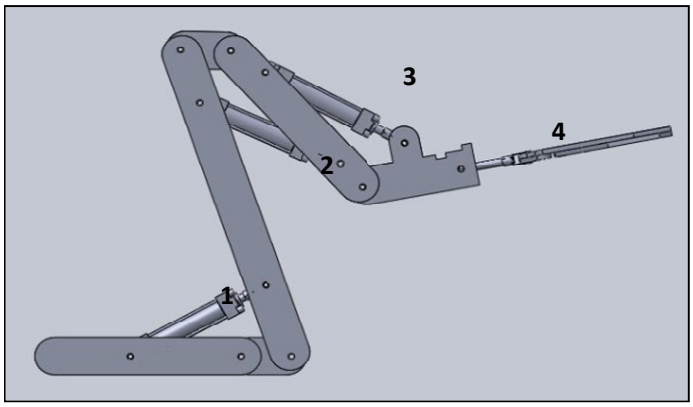

Fig. 4. A Manipulator in the Retracted Position

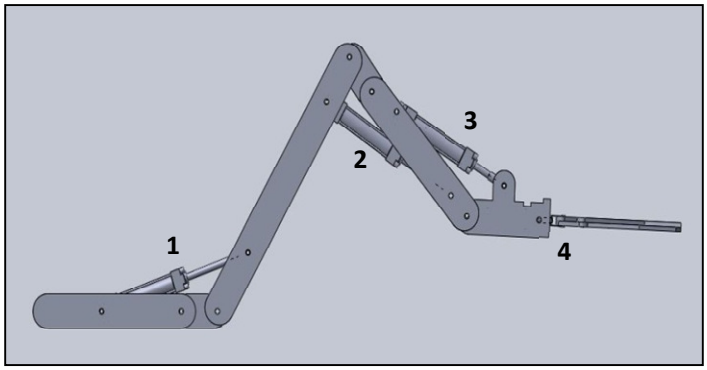

Fig. 5. A Manipulator in the Extended Position

Table 2
Preset Angle for CFD Simulation

Angle	Retracted Manipulator	Extended Manipulator
θ_1	90°	130°
θ_2	90°	130°
θ_3	107.5°	120°
θ_4	107.5°	130°

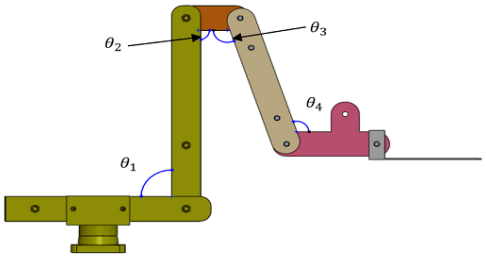

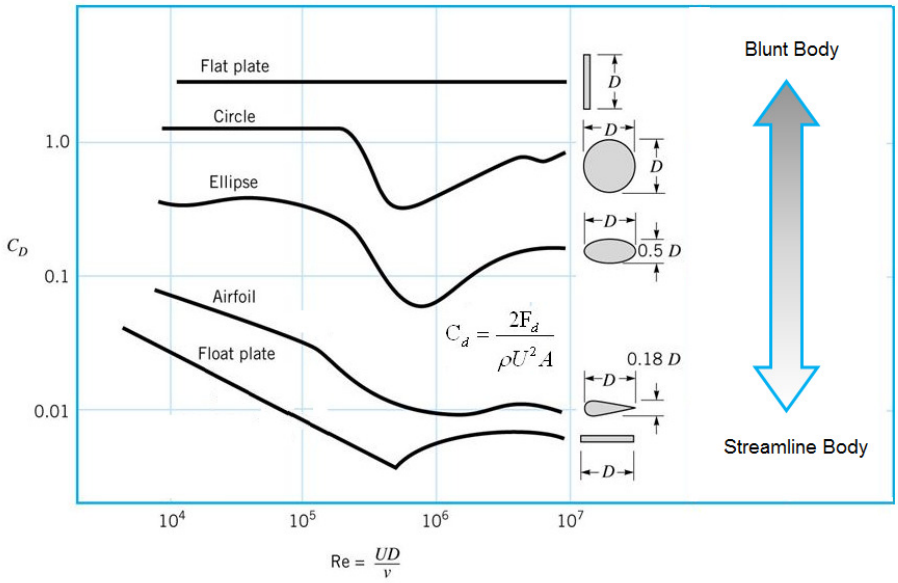

Fig. 6. Streamline and Blunt Body Characteristics [14]

3. Kinematics Analysis of Four Joints Manipulator

Underwater manipulators consist of rigid links connected in series by pin joints. The joint torques for generating the motion of the links have to overcome the weight and payload along with the hydrodynamic load induced by relative motion of the arm and the fluid. Four joints, each driven by a linear actuator is used in the manipulator design. Each actuator or cylinder has double acting configuration, and is able to sustain a maximum extension of 125 cm, with bore size of 40 cm. The manipulator is made up of a series of segments and joints that connect four segments together and allow them to move relative to one another. The joints provide either linear (straight line) or rotary (circular) movement. Fives valves are used to control the movement of five cylinders, as shown in Figure 7. The operator manipulates the actuator by changing the switching position of the valves. Kinematics analysis for multi-degree of freedom of the manipulator arm connects the relationship between each link and connectivity which involve the value of motion angle, workspace and to define the gripper or the end-effector for certain configuration of manipulator arm without considering any contributing force. The analysis applies the concept of trigonometry equation in order to determine the parameters between each point in connected link which form the certain value of angle. Inverse kinematics analysis is used to provide a desired position of the gripper by the required joint angles.

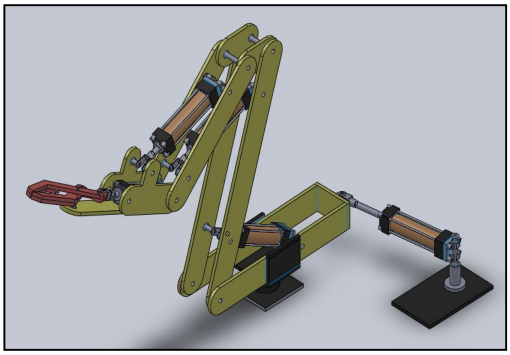

Fig. 7. Manipulator Arm Full Assembly

In Figure 8 and 9, the kinematic analysis for angle in between link AB and BC can be denoted as

$$\alpha B = cos^{-1}\left(\frac{(AB)^2+(BC)^2-(AC)^2}{2(ABxBC)}\right) \quad (1)$$

and,

$$\theta B = 180 - \alpha B \quad (2)$$

where αB= degree of angle for AC and θB = degree of angle against x axis. For link CD and DE, the angle can be denoted as

$$\alpha D = cos^{-1}\left(\frac{(CD)^2+(DE)^2-(CE)^2}{2(CDxDE)}\right) \quad (3)$$

and,

$$\theta D = 180 + \alpha D \quad (4)$$

where αD = degree of angle CE and θD = degree of angle against x axis. The angle in between link EF and FG can be denoted as

$$\alpha E = cos^{-1}\left(\frac{(DE)^2+(EF)^2-(DF)^2}{2(DExEF)}\right) \quad (5)$$

and,

$$\theta E = 180 - \alpha E \quad (6)$$

where αE = degree of angle CE and θE = degree of angle against x axis. In Figure 10 and 11, the angle in between link ABC, which is controlled by the movement of cylinder 1 can be represented by

$$\alpha B = cos^{-1}\left(\frac{(AB)^2+(BC)^2-(AC)^2}{2(ABxBC)}\right) \quad (7)$$

and,

$$\theta B = 180 - \alpha B \quad (8)$$

where AC = cylinder displacement, αB = degree of angle AC and θB = degree of angle against x axis. For cylinder 2, the kinematic analysis will involve link DEF and DFG, where

$$\alpha F_1 = cos^{-1}\left(\frac{(DF)^2+(EF)^2-(DE)^2}{2(DF\times EF)}\right) \quad (9)$$

and,

$$\alpha F_2 = cos^{-1}\left(\frac{(DF)^2+(FG)^2-(DG)^2}{2(DF\times FG)}\right) \quad (10)$$

and,

$$\theta F = 180 + \alpha F_1 + \alpha F_2 \quad (11)$$

where DF = cylinder displacement, αF_1 = degree of angle DE and αF_2 = degree of angle DG and θF = degree of angle against x axis. The movement of cylinder 3, which represent link HIJ can be denoted as

$$\alpha I = cos^{-1}\left(\frac{(HI)^2+(IJ)^2-(HJ)^2}{2(HIxIJ)}\right) \quad (12)$$

and,

$$\theta I = 180 - \alpha I \quad (13)$$

where HJ = cylinder displacement, αI = degree of angle HJ and θI = degree of angle against x axis. The workspace area of the manipulator arm is also defined as the working area of the end-effector. In other words, workspace is the minimum and maximum distance of the end-effector that can be reached. Workspace analysis of this project the in x-axis and y-axis as shown Figure 12.

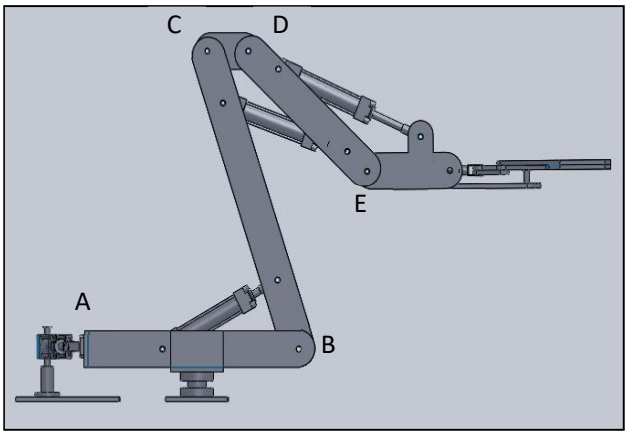

Fig. 8. Retracted Manipulator with Link of AB, BC, DE and EF

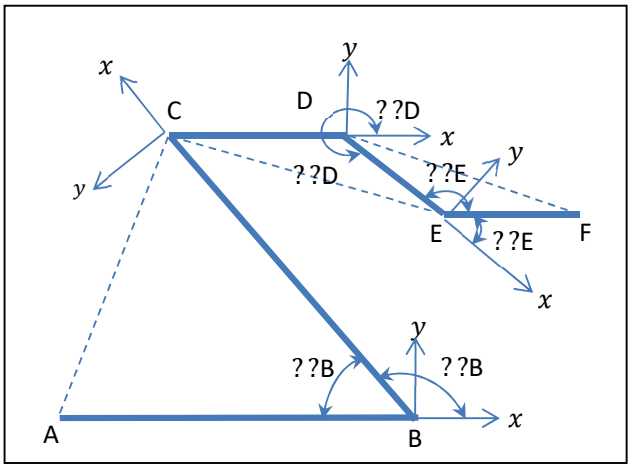

Fig. 9. Kinematic Analysis for Each Link of AB, BC, DE and EF

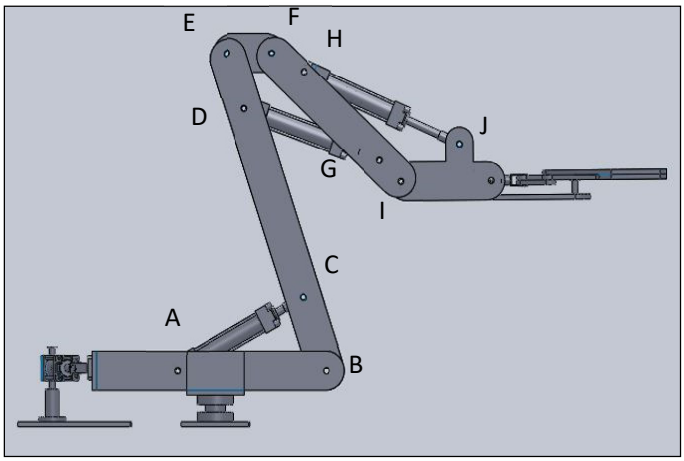

Fig. 10. Retracted Manipulator with Link based on Cylinder Displacement

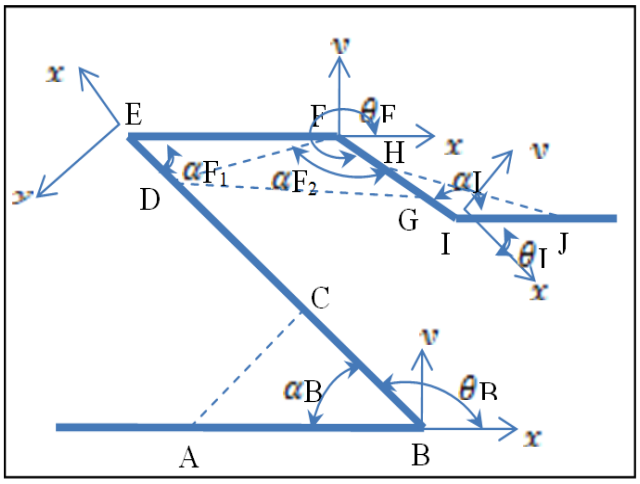

Fig. 11. Kinematic Analysis for Each Link based on Cylinder Displacement

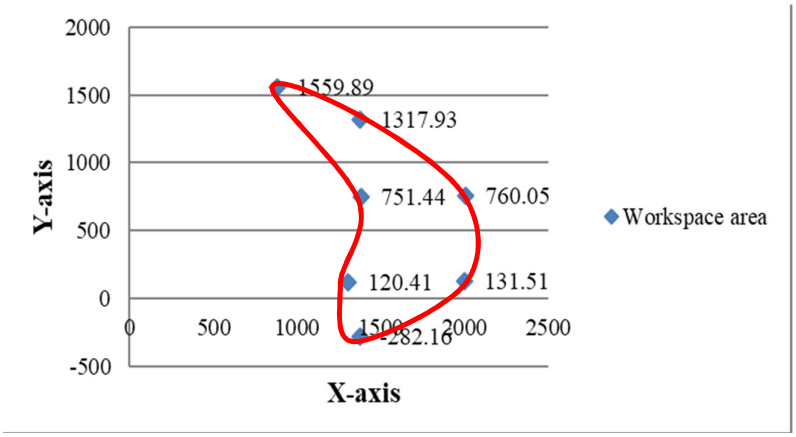

Fig. 12. Workspace Area of the End-effector

4. Computational Fluid Dynamics Analysis

The design of the manipulator arm that is being used in the CFD analysis involve several parts with joints. The cylinders or linear actuators for the manipulator arm have been neglected to simplify the analysis. The prototype manipulator arm is sketched manually, before being transferred to computer aided design software [16]. The manipulator arm in the CFD analysis has five degrees of freedom. Parameter has been set for the analysis which is using water and air as the medium and laminar flow model with velocity 0.1 m/s. The meshing result of the manipulator within the setting of the boundary domain of 4.8m^3 volume around it. The meshing is done by using CutCell method for cubical mesh features with minimum sizing $1x10^{-4}$ m, and curvature angle of 18^o. The total node for the mesh result is 3,384,282 nodes. The simulation have been set for operating pressure of 0 Pa to cut down the rounding errors and limit the boundary pressure. Absolute viscosity of air and water is set at 1.846 x 10^{-5} and 8.53 x 10^4 kgm/s at room temperature of 300K, while their density is set at 1.161 and 996.57 kg/m^3.

4.1 Pressure Distribution in the Retracted Position

The result from the analysis shown in Figure 13, where the manipulator is simulated in a suspended and retracted position, the highest pressure was about $8.49x10^{-3}$ Pa on the area which is cylindrical shape linker, middle arm, a small area at tips of the gripper holder and base of the simulated manipulator. Middle range pressure occurs on the side arm thickness area that directly exposed to flow direction which around$-6.02x10^{-4}$ to $3.19x10^{-3}$ Pa. The lower pressure occurs on the model is in range between $-6.66x10^{-3}$ to $-2.12x10^{-3}$ Pa along at the side of the middle arm. The base and prototype back sheet plate having middle range pressure. Since the simulation have been set for operating pressure of 0 Pa to cut down the rounding errors, negative pressure has been detected in the simulation. In the Navier-Stokes equations, pressure differences is the key element that drives the flow. Since the flow get separated, the low pressure inside that region will be relative to the lowest fixed pressure in the system and thus providing negative value. In Figure 14, the manipulator is simulated as a submerged streamline body in the water, with rectracted position. The highest pressure is about 5.61 Pa , occur on cylindrical shape linker, middle arm, a small area at tips of the gripper holder and base of the manipulator. Middle range pressure occurs dominantly which mostly on the side arm thickness area that directly exposed to flow direction which around −2.32 to $3.21x10^{-1}$ Pa. The lower pressure occur on the model is in range between −7.61 to−3.65 Pa back of the cylindrical shape linker. Base and the back-sheet plate of the prototype having high pressure within 1.64 to 4.29 Pa.

From Figure 15, the direction of the flow direction is set along the x-axis. This changes the condition of the manipulator from streamline body to blunt body. As expected, pressure distribution is high in this position, where the highest pressure reaches $8.21x10^{-3}$ Pa on all the arm part expose to flow in the x-axis. It is to be noted that, the manipulator is in suspended mode, where the simulated fluid resembles the properties of air. Middle range pressure occurs mostly on gripper holder and the base which is between $-2.02x10^{-3}$ to $1.39x10^{-3}$ Pa. The dominant pressure occur on the prototype is in range between $-5.81x10^{-3}$ $to$$-3.91x10^{-3}$ Pa. Lowest pressure occur at $-1.07x10^{-2}$ Pa. In the submerged mode, with water property, the highest pressure is about 6.21 Pa all over the arm along the exposed part to flow direction on x-axis, as shown in Figure 16. Middle range pressure occurs mostly on gripper holder or the end-effector, and the base which is between −2.41 to 1.24 Pa. The dominant pressure occur on the prototype is in range between −6.73 to −3.74 Pa. Lowest pressure occurs at −10.4 Pa.

4.2 Pressure Distribution in the Extended Position

From the suspended, extended streamline manipulator, where the analysis is conducted based on the property of air, the pressure distribution result is shown in Figure 17, where the highest pressure is about $8.96x10^{-3}$ Pa on the area such as cylindrical shape linker, middle arm and base of the simulated manipulator. Middle range pressure occurs on the side arm thickness, the third part of short arm section and the gripper/end-effector which is in between $2.63x10^{-3}$ to $4.63x10^{-3}$Pa. The lower pressure mostly occurs on the manipulator in between $-7.03x10^{-4}$ to $1.30x10^{-3}$Pa along at the side of the middle arm. Lowest pressure occurs at the base which is $-7.70x10^{-3}$Pa.

In the submerged scenario mode, as shown in Figure 18, the highest pressure is about 5.47 Pa, which occurs on the cylindrical shape linker, middle arm, a small area at tips of the gripper holder and base of the extended streamline manipulator. Middle range pressure occurs dominantly along the arm which from $-3.27x10^{-1}$ to 1.93 Pa. The lower pressure occur on the model is in range between $-1.06x10^{1}$ to −5.16 Pa back of the cylindrical shape linker. Base and the back-sheet plate of the manipulator have highest pressure within 1.93 to 3.86 Pa, since the plate resemble part of the blunt body area.

Figure 19 shows the suspended, extended blunt manipulator, where the highest pressure is about $7.62x10^{-3}$ Pa all over the exposed arm part to the x-axis flow direction. Middle range pressure occurs mostly on gripper holder, edge of arm and the base which is between $-1.21x10^{-3}$ to $2.33x10^{-3}$ Pa. The dominant pressure occurs on the manipulator within range between $-6.06x10^{-3}$ to $-2.09x10^{-3}$ Pa. Lowest pressure is $-1.45x10^{-2}$ Pa occurring within small area.

The highest pressure was about 5.78 Pa on the entire arm along the expose part to x-axis flow direction, as shown in Figure 20. The manipulator is set to be in a submerged, blunt and extended position setup. Middle range pressure occurs mostly on gripper holder and the base which is between−2.52 to 1.44 Pa. The dominant pressure occur on the manipulator is in range between −5.68 to −2.91 Pa. The lowest pressure occurs at $-1.4x10^{1}$ Pa.

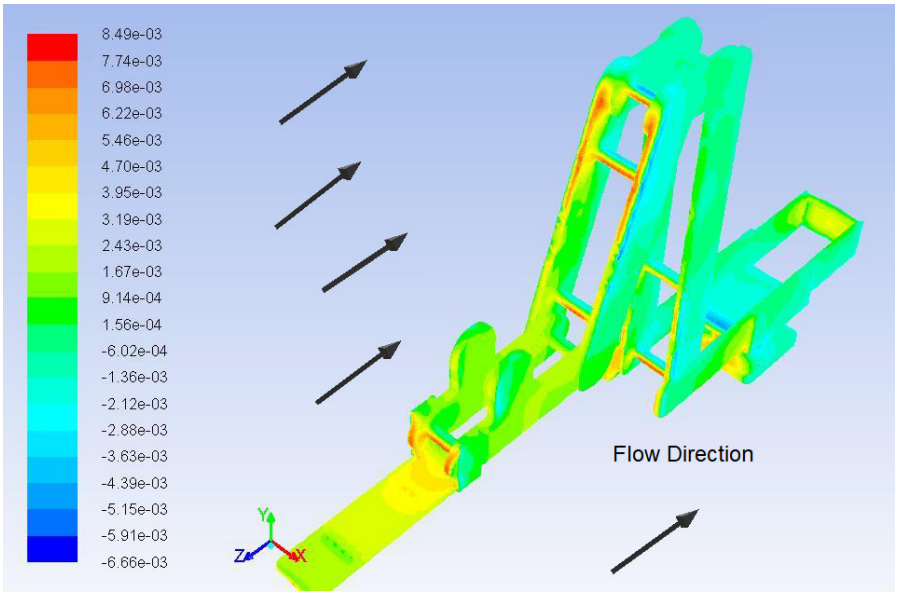

Fig. 13. Pressure Distribution Analysis for Suspended, Retracted Streamline Manipulator Setup

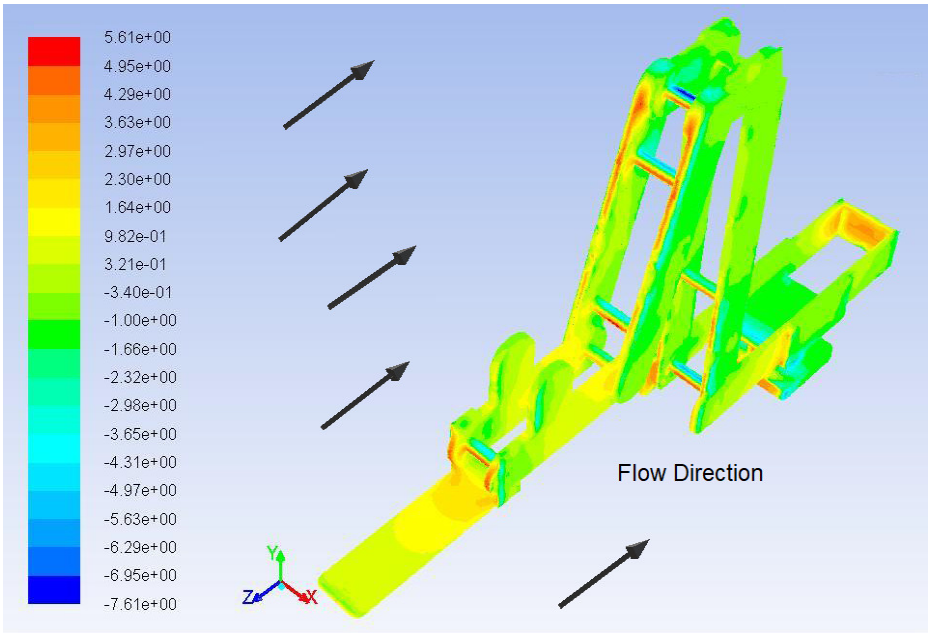

Fig. 14. Pressure Distribution Analysis for Submerged, Retracted Streamline Manipulator Setup

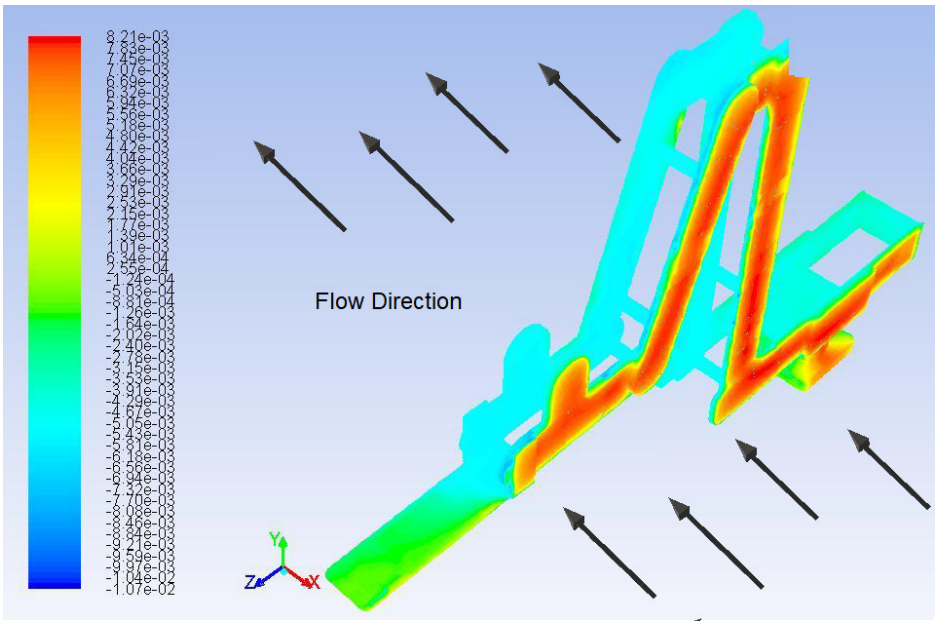

Fig. 15. Pressure Distribution Analysis for Suspended, Retracted Blunt Manipulator Setup

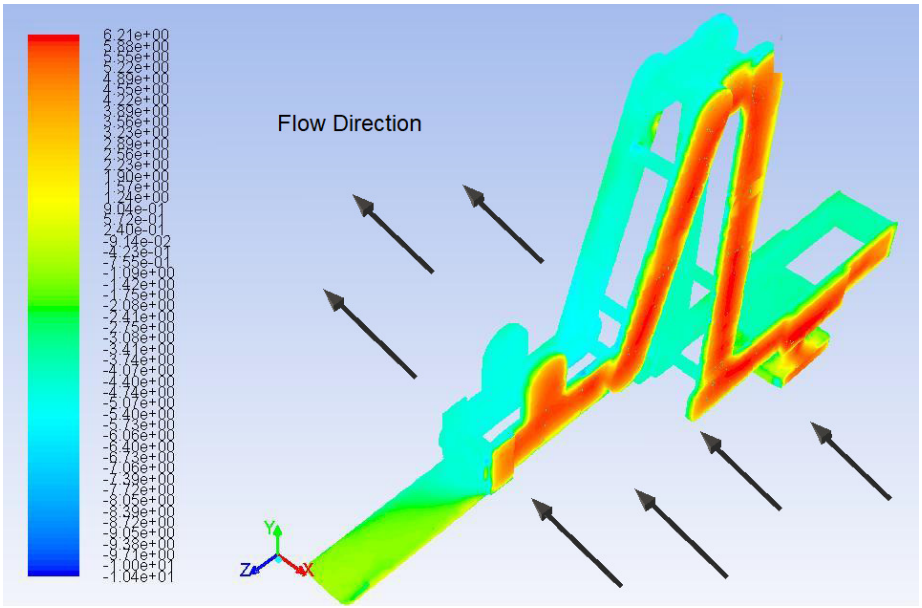

Fig. 16. Pressure Distribution Analysis for Submerged, Retracted Blunt Manipulator Setup

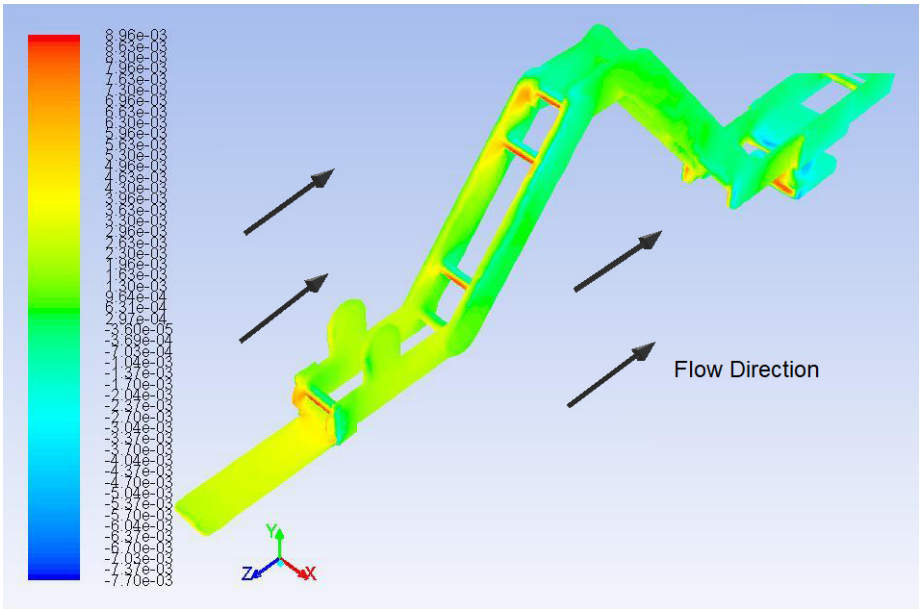

Fig. 17. Pressure Distribution Analysis for Suspended, Extended Streamline Manipulator Setup

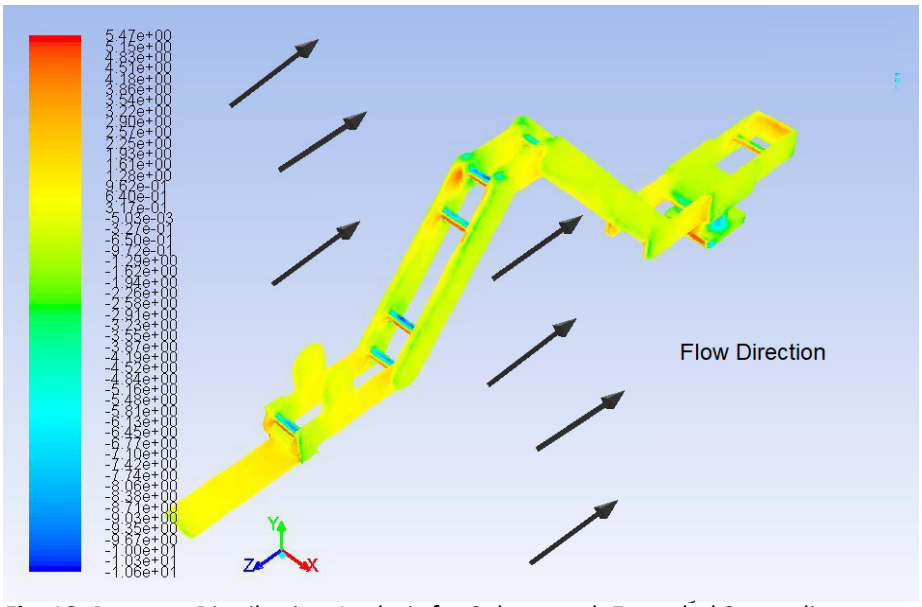

Fig. 18. Pressure Distribution Analysis for Submerged, Extended Streamline Manipulator Setup

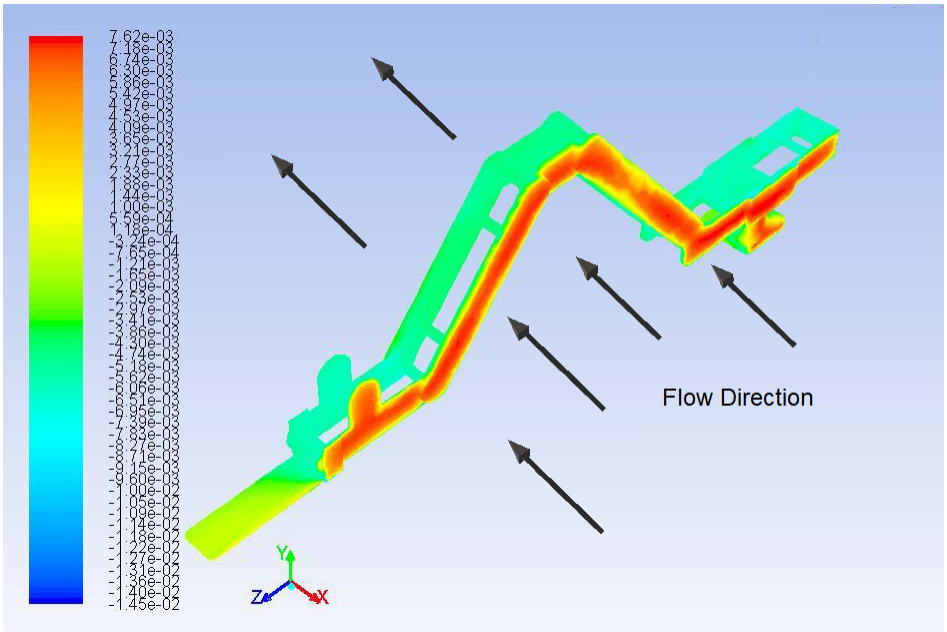

Fig. 19. Pressure Distribution Analysis for Suspended, Extended Blunt Manipulator Setup

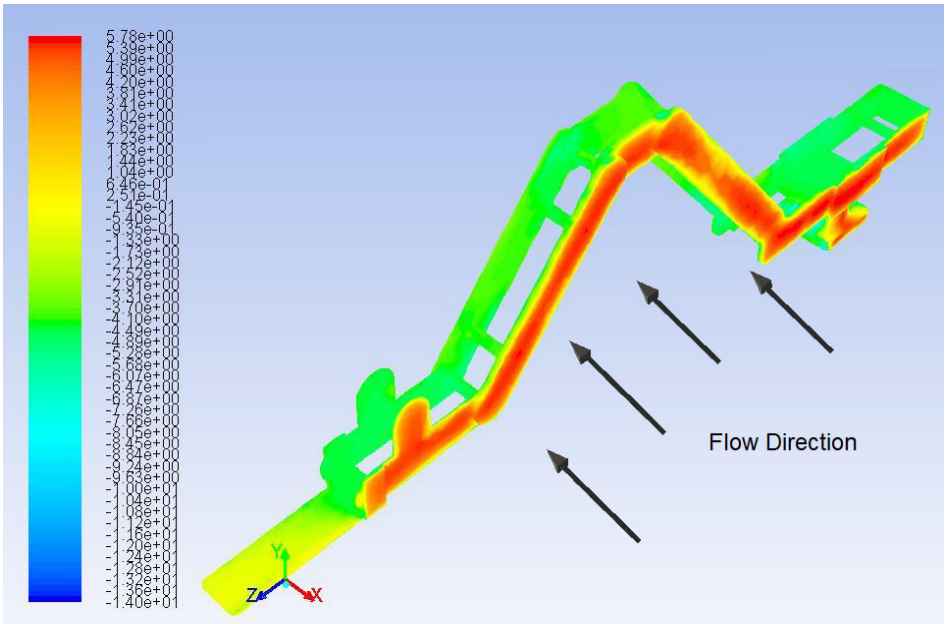

Fig. 20. Pressure Distribution Analysis for Submerged, Extended Blunt Manipulator Setup

4.3 Velocity Vector in Retracted Position

From the velocity vector shown in Figure 21, the small area of gripper holder tip and most of the arm joint area have low velocity between 2.93×10^{-5} to 4.06×10^{-2} m/s. The manipulator in this figure is simulated in a suspended and retracted position, with the property of air. Small vectors of high velocity which range 9.47×10^{-2} to 1.35×10^{-1} m/s occur at the side of arm thickness. The velocity is between the range of 6.09×10^{-2} to 8.79×10^{-2} m/s at the end-effector.

Figure 22 shows the velocity vector when the manipulator is simulated as a submerged streamline body in the water, with rectracted position. Existence of low velocity vector is noted at the small area of gripper/end-effector holder tip and most of the arm joint area between 4.63×10^{-2} to 4.73×10^{-4} m/s. Vector of high velocity range from 9.98×10^{-2} to 1.38×10^{-1} m/s occurs at the side of arm thickness. The top of gripper velocity is between 6.92×10^{-2} to 9.98×10^{-2} m/s. The highest velocity occurs behind the cylindrical shape linker which is around $1.53x10^{-1}$ m/s.

Figure 23 shows the suspended, retracted blunt manipulator velocity vector, which is facing flow direction along the x-axis. The dominant velocity occurs between 2.12×10^{-5} to 3.23×10^{-2} m/s. Velocity occurs on the gripper holder mostly have the region of yellow and orange indicator with velocity range of 9.39×10^{-2} to 1.29×10^{-1} m/s. Highest velocity occur is 1.47×10^{-1} m/s within a small area.

In the simulated submerged mode, Figure 24 shows a dominant velocity which occurs between 1.71×10^{-4} to 4.60×10^{-2} m/s. Velocity of 9.80×10^{-2} to 1.29×10^{-1} m/s occurs on the gripper holder. Highest velocity occurs at 1.53×10^{-1} m/s within a small area at the base.

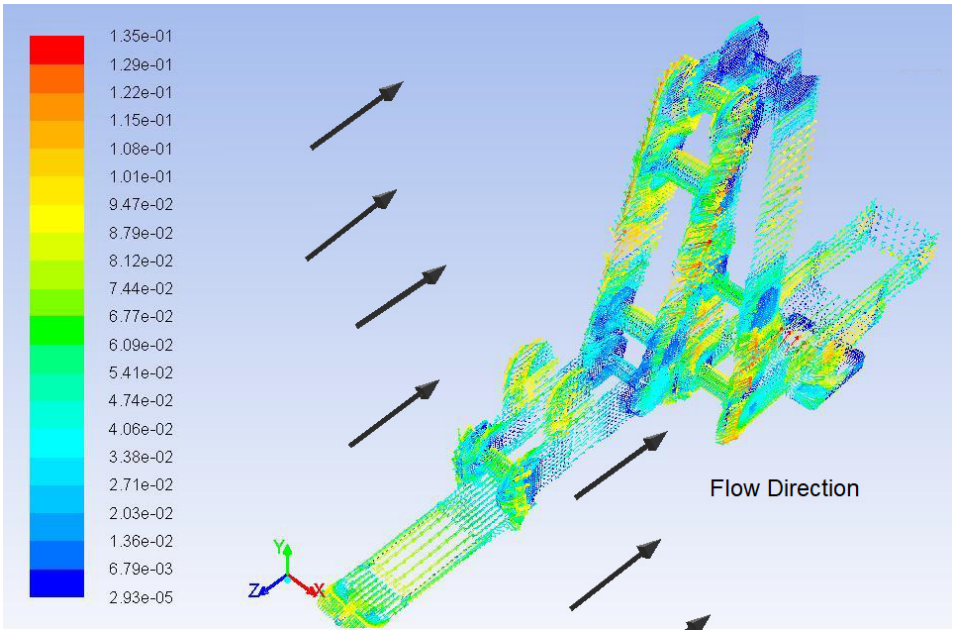

Fig. 21. Velocity Vector Analysis for Suspended, Retracted Streamline Manipulator Setup

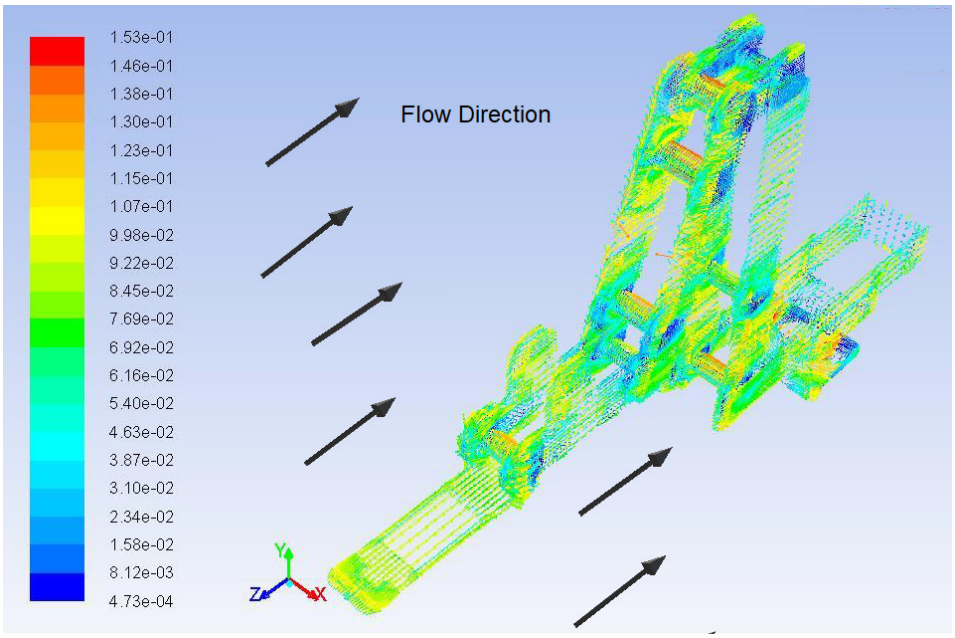

Fig. 22. Velocity Vector Analysis for Submerged, Retracted Streamline Manipulator Setup

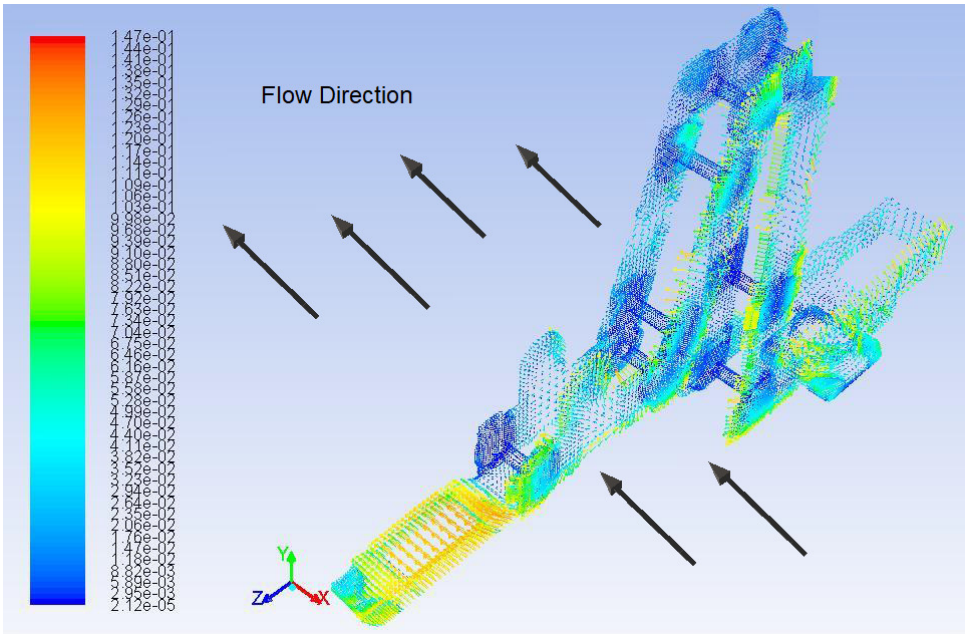

Fig. 23. Velocity Vector Analysis for Suspended, Retracted Blunt Manipulator Setup

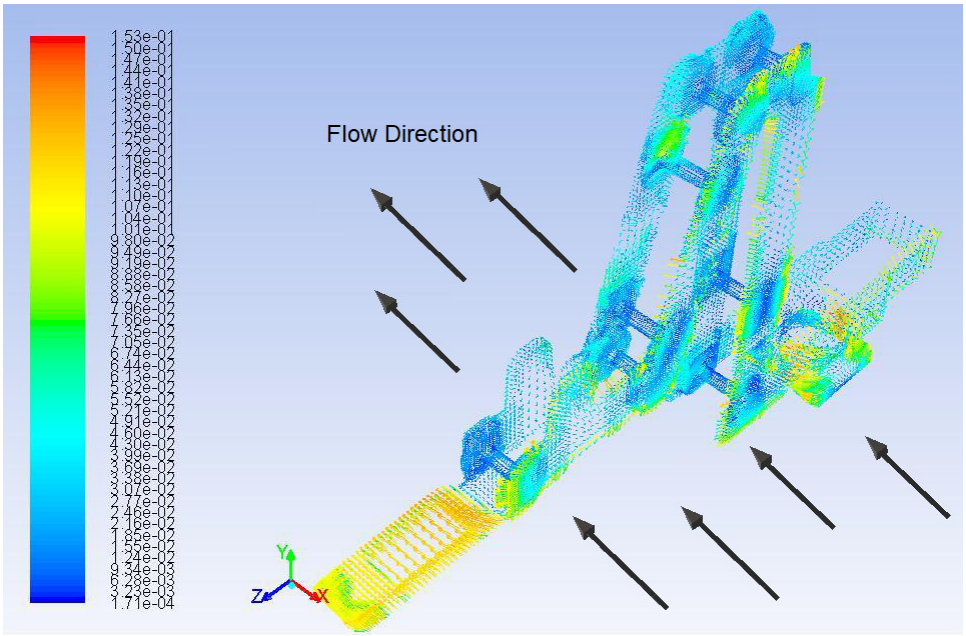

Fig. 24. Velocity Vector Analysis for Submerged, Retracted Blunt Manipulator Setup

4.4 Velocity Vector in Extended Position

Figure 25 shows the suspended, extended streamline manipulator, where low air velocity is simulated between 1.63×10^{-5} to 3.00×10^{-2} m/s. A small area of high velocity which range 6.91×10^{-2} to 1.20×10^{-1} m/s occurs at the side of arm thickness. On top of the gripper holder, velocity is in between 3.90×10^{-2} to 5.71×10^{-2} m/s.

For the submerged manipulator in Figure 26, the velocity vector shows the low velocity occurrence at the small area of gripper holder tip and most of the arm joint area between 4.63×10^{-2} to 4.73×10^{-4} m/s. High velocity range from 9.68×10^{-2} to 1.43×10^{-1} m/s occurs at the side of arm thickness. The top of gripper velocity is between 6.81×10^{-2} to 8.60×10^{-2} m/s. Highest velocity occurs behind the cylindrical shape linker which is $1.79x10^{-1}$ m/s.

From the velocity vector shown in Figure 27, the dominant velocity occurs between 3.83×10^{-6} to 4.57x10-2 m/s. The velocity which occurs on the gripper holder has a region of velocity range between 8.43×10^{-2} to 1.23×10^{-1}m/s. Highest velocity occurs at 1.76×10^{-1} m/s within a small area.

Velocity vector analysis for submerged, extended blunt manipulator setup is shown in Figure 28. The velocity occurs between the range of 1.56×10^{-5} to 5.33×10^{-2} m/s. The velocity that occurs on the gripper holder has a range of 9.90×10^{-2} to 1.33×10^{-1} m/s. Highest velocity occurs at 1.90×10^{-1} m/s within a small area at the base.

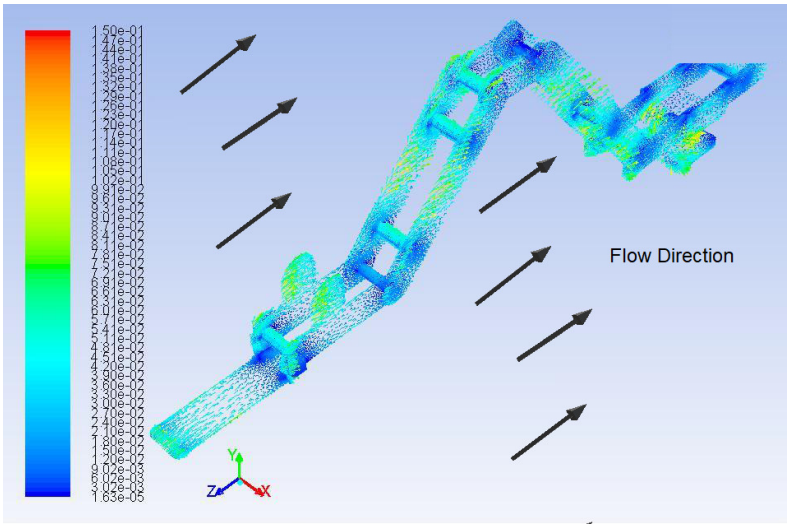

Fig. 25. Velocity Vector Analysis for Suspended, Extended Streamline Manipulator Setup

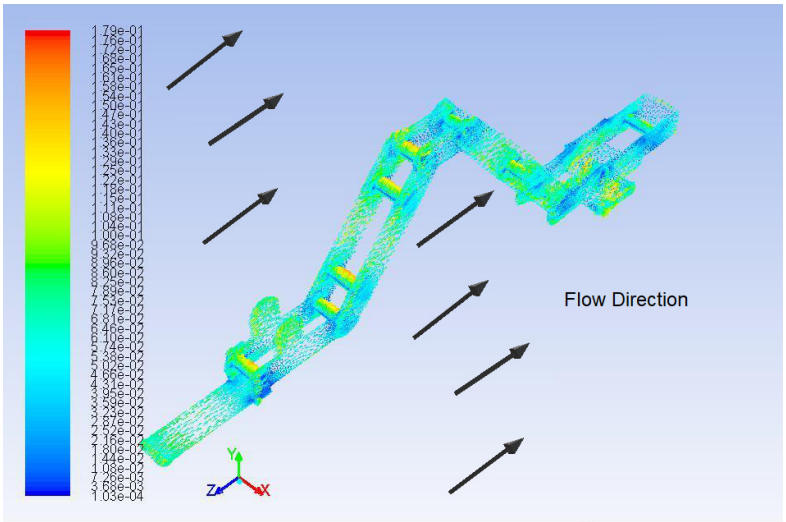

Fig. 26. Velocity Vector Analysis for Submerged, Extended Streamline Manipulator Setup

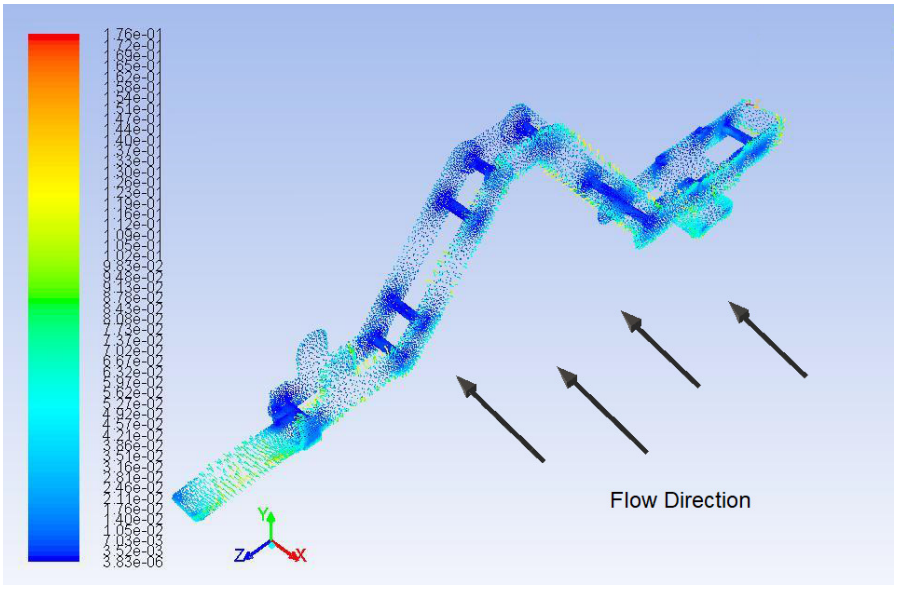

Fig. 27. Velocity Vector Analysis for Suspended, Extended Blunt Manipulator Setup

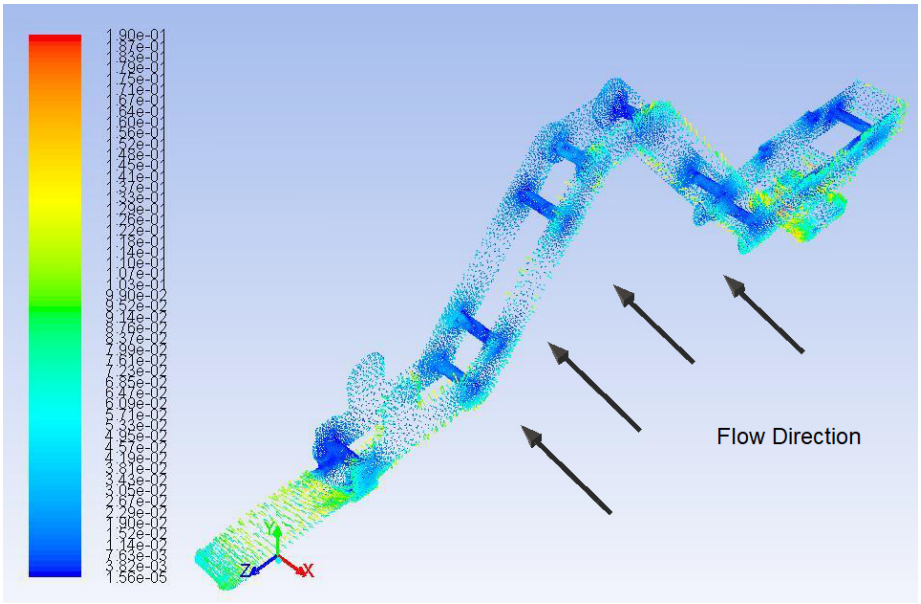

Fig. 28. Velocity Vector Analysis for Submerged, Extended Blunt Manipulator Setup

5. Conclusions

A kinematic and dynamic analysis has been conducted for an underwater manipulator. The manipulator has been designed with four joints, each driven by a linear actuator, to analyze the effectiveness of the system for underwater application. Kinematic analysis of the manipulator reveals the possible workspace area for the system. A computational fluid dynamic analysis is also conducted to observe the effect of fluid flow and relative flow direction on the pressure distribution and velocity vector of the manipulator. The surrounding medium has been set to of water and air, to mimic the function of the manipulator under and above the water. Parameters for the analysis has been set for

laminar flow condition, with low velocity at 0.1 m/s. It is anticipated that the value is suitable for underwater applications. The manipulator arm model is defined as a static body in a moving fluid. High pressure is noted to occur at the arm, the tips of the gripper holder and model base as it exposed to the fluid flow and velocity. High pressure distribution is noted for most of blunt body setup. The results show that high pressure distribution occurs when the manipulator is subjected to side flow. In this scenario, the flat surface area should be reduced, so that low drag will occur. Typical solution is to introduce a long hole, for low drag solution. The manipulator should be redesigned with a different type of surface area, for a better hydrodynamic performance.

Acknowledgements
This work was funded by Ministry of Higher Education (MOHE) of Malaysia, under the Fundamental Research Grant Scheme (FRGS). FRGS/1/2016/TK03/FKM-CARE-F00317. The authors wish to thank Mr. Muhammad Zul Fikri Suhaimi and Mr. Muhammad Faiz Othman for their contribution in the simulation and analysis of the project.

References

[1] Kraft, Brett W. "Underwater manipulator system." *U.S. Patent No. 4648782*. Washington, DC: U.S. Patent and Trademark Office, 2003.
[2] Ahmad Anas Yusof, Faizil Wasbari and Mohd Qadafie Ibrahim. "Research Development of Energy Efficient Water Hydraulics Manipulator for Underwater Application."*Applied Mechanics and Materials*, 393, (2013): 723 –728.
[3] Tadahiro Hyakudome. "Design of Autonomous Underwater Vehicle." *International Journal of Advanced Robotic Systems*, Vol. 8, No. 1, (2011): 122 – 130.
[4] Hiroshi Yoshinada, Taku Yamazaki, Tatsunori Suwa, Toshihisa Naruse and H. Ueda. "Seawater Hydraulic Actuator System for Underwater Manipulator." *Proceeding of the 5th International Conference on Advanced Robotics*, Pisa, Italy, (1991). 1330 – 1335.
[5] Hassan, Siti Nor Habibah, Ahmad Anas Yusof, Tee Boon Tuan, Mohd Noor Asril Saadun, Mohd Qadafie Ibrahim, and Wan Mohd Norsani Wan Nik. "Underwater manipulator's kinematic analysis for sustainable and energy efficient water hydraulics system." In *AIP Conference Proceedings*, vol. 1660, no. 1, p. 070112. AIP Publishing, 2015.
[6] Kołodziejczyk, Waldemar. "Some considerations on an underwater robotic manipulator subjected to the environmental disturbances caused by water current." *acta mechanica et automatica* 10, no. 1 (2016): 43-49.
[7] Rahman, Irfan Abd, Surina Mat Suboh, and Mohd Rizal Arshad. "Theory and design issues of underwater manipulator." In *Presented at Int. Conf. Control, Instrumentation and Mechatronics Engineering (CIM'07)*. 2007.
[8] Denavit J. and Hartenberg, R.S. "A kinematic notation for lowerpair mechanisms based on matrices." *Trans ASME J. Appl. Mech*, 23, (1955):215 – 221.
[9] Hartenberg, Richard Scheunemann, and Jacques Denavit. *Kinematic synthesis of linkages*. McGraw-Hill, 1964.
[10] Li, Ruiheng, Amir Parsa Anvar, Amir M. Anvar, and Tien-Fu Lu. "Dynamic modeling of underwater manipulator and its simulation." In *Proceedings of World Academy of Science, Engineering and Technology*, no. 72, p. 27. World Academy of Science, Engineering and Technology (WASET), 2012.
[11] McLain, Timothy W., and Stephen M. Rock. "Development and experimental validation of an underwater manipulator hydrodynamic model." *The International Journal of Robotics Research* 17, no. 7 (1998): 748-759.
[12] Santhakumar, Mohan. "Investigation into the dynamics and control of an underwater vehicle-manipulator system." *Modelling and Simulation in Engineering* 2013 (2013): 17.
[13] Filaretov, V. F., and A. Yu Konoplin. "System of Automatically Correction of Program Trajectory of Motion of Multilink Manipulator Installed on Underwater Vehicle." *Procedia Engineering* 100 (2015): 1441-1449.
[14] Munson, Bruce R., Donald F. Young, Theodore H. Okiishi, and Wade W. Huebsch. "Fundamentals of fluid mechanics. Hoboken." *John Wiley & Sons, Inc* 69 (2006): 520.
[15] Suhaimi, Muhammad Zul Fikri. "The Analysis of Fluid Structure Interaction for Submersible Water-hydraulic Manipulator Using Computational Fluid Dynamics." PhD diss., Universiti Teknikal Malaysia Melaka, 2015.
[16] Muhammad Faiz , Othman. (2013). The design and fabrication of hydraulic boom trainer with gripper attachment. Project Report. UTeM, Melaka.